SEENS: Nuclei Segmentation in Pap Smear Images with Selective Edge Enhancement*

Meng Zhao[a,b,*,1], Hao Wang[b,*], Ying Han[a], Xiaokang Wang[c], Hong-Ning Dai[d], Xuguo Sun[e], Jin Zhang[f] and Marius Pedersen[b]

[a]Key Laboratory of Computer Vision and System of Ministry of Education, School of Computer Science and Engineering, Tianjin University of Technology, China
[b]Department of Computer Science, Norwegian University of Science and Technology, Norway
[c]Department of Computer science, St. Francis Xavier University, Canada
[d]Faculty of Information Technology, Macau University of Science and Technology, Macau
[e]School of Medical Laboratory, Tianjin Medical University, China
[f]College of Electrical Engineering, Sichuan University, China

ARTICLE INFO

Keywords:
Nuclei segmentation
Selective search
Selective edge enhancement
Canny operator
Chan-Vese model

ABSTRACT

Accurate nuclei segmentation, as an indispensable basis and core link for multi-cell cervical image analysis, plays an important role in automatic pre-cancer detection. However, poor image quality due to the uneven staining, complex backgrounds and overlapped cell clusters poses a great challenge in nuclei segmentation. In this paper, we propose a new Selective-Edge-Enhancement-based Nuclei Segmentation method (SEENS). In the proposed method, selective search is integrated with mathematical operators to segment whole slide cervical images into small regions of interest (ROI) while automatically avoiding repeated segmentation as well as eliminating non-nuclei regions. In addition, an edge enhancement method based on the canny operator and mathematical morphology is presented to extract edge information as a weight to enhance the nucleus edge selectively. As a result, the enhanced ROI is then segmented by the Chan-Vese model with a higher accuracy. We evaluate our method with 18 whole slide images for a total of 395 cell nuclei. Experimental results demonstrate that SEENS achieves higher accuracy in cervical nuclei segmentation. Notably our method performs particularly better in low-contrast scenarios than baselines.

1. Introduction

Cervical cancer is one of the most common gynecologic malignancies. In recent years, the incidence of cervical cancer has been increasing year by year, and the age of onset tends to be younger. Therefore, the prevention and treatment of cervical cancer have become a hot topic in academia. Driven by the fourth revolution in healthcare technologies [1, 2], led by the boom of Big Data [3, 4] and Machine Learning/Deep Learning [5, 6, 7], Health engineering is emerging as a new interdisciplinary field of research and development [8, 9]. This may lead to a revolutionized healthcare system that enables the participation of all people for the early detection and prevention of diseases. In this manner, preemptive and proactive treatments can be delivered to realize the personalized, pervasive, and patient-centralized healthcare.

At present, cervical cytology screening has been widely used, so that the cervical cancer and precancerous lesions can be detected and treated early, thereby significantly decreasing the morbidity and mortality of cervical cancer. Among numerous cervical cancer screening methods, Pap smear [10, 11] has been considered one of the most effective methods of cytology testing for early screening of cervical cancer. The essence of cervical cancer screening based on Pap smear is to extract and analyze the characteristics of cells or nuclei. As the basic step of quantitative analysis of cell or nucleus morphology, image segmentation [12, 13] plays a core role because the accuracy of the segmentation directly affects the correctness of analysis results.

*This document is the results of the research project funded by the National Science Foundation of China (Grant Nos. 61703304, 61906133 and U1509207), R & D Plan in Key Field of Guangdong Province (Grant No. 2019B010109001), Major Science and Technology Projects of Tianjin (Grant No.18ZXZNGX00150) and is carried out with the support of ERCIM 'Alain Bensoussan' Fellowship Programme.".

*Corresponding authors
zh_m@tju.edu.cn (M. Zhao); hawa@ntnu.no (H. Wang)
ORCID(s): 0000-0002-5060-9223 (M. Zhao); 0000-0001-9301-5989 (H. Wang)

1.1. Related work

There are many cell or nuclei image segmentation methods, which can be generally divided into three categories.

First, cell or nucleus segmentation methods adopt region information to classify each pixel in an image. Typical nucleus segmentation methods include threshold methods [14, 15], region growing [16, 17], clustering [18, 19] and watershed algorithms [20, 21, 22].

Second, segmentation methods using cell or nucleus edge information utilize the discontinuity of gray information to segment the image; they mainly include differential operator methods and active contour models [23, 24, 25, 26, 27].

Third, cell or nucleus segmentation methods are mainly based on related theories [28, 29], such as wavelet analysis [30, 31], mathematical morphology [32, 33, 34], genetic algorithm [35] and neural networks [36, 37, 38].

In addition, many state-of-the-art cell or nuclei segmentation algorithms are no longer based on a single algorithm but multiple algorithms together, namely, fusion algorithms, which aim to make up for the shortage of a single algorithm and achieve better segmentation results [39, 40].

Due to the differences of slice-making and staining techniques, the quality of cervical smears is varied (either good or bad), e.g., uneven staining and complex background of the smear images. In addition, both irregular cervical cell shape and overlapping cells bring difficulties in the direct segmentation of whole cervical cells.

For the highly-overlapping cell clusters, only first segmenting and then analyzing cervical nuclei can also be used for cervical cancer screening. On one hand, nuclei of cancer cells contain most of the features of pathological changes. Thus, quantitative analysis of nucleus morphology is reliable while it does not affect the cervical cancer cells screening results. On the other hand, it reduces the difficulty of segmentation and simplifies the operation process.

Therefore, many classical algorithms have been developed for cervical nucleus segmentation. For instance, Plissiti et al. [41] used morphological reconstruction and clustering to detect cell nuclei from region of interest (ROI) produced by the Otsu threshold method. Zhang et al. [42] combined fully convolutional networks with a graph-based approach for segmentation of cervical nuclei. Plissiti et al. [43] presented a two-step fully-automated method for the segmentation of the nuclei. In the first stage, based on a morphological image reconstruction process, locations of nuclei were detected. In the second stage, the watershed transform was applied to the morphological color gradient image to segment nuclei boundaries. Byju et al. [44] used a customized Laplacian of Gaussian filter to detect the edge of nucleus and then segment the nucleus. Song et al. [45] proposed a method for segmentation of cervical cytoplasm and nuclei; this method combines a multi-scale convolutional network with graph partitioning. Muhimmah et al. [46] utilized morphological operations and watershed transformation to segment nuclei. Chang et al. [47] proposed a nucleus detection algorithm using mean shift and the energy method. Zhang et al. [48] presented a global and local scheme based on graph cut for segmentation of cytoplasm and nuclei.

Most of the algorithms aforementioned perform the segmentation directly on the original image, which may result in the loss of the cell nuclei with low-intensity contrast. As shown in Fig. 1, the unclear boundaries of the nuclei with poor contrast against the cytoplasm makes it more difficult to achieve precise segmentation results. Guan et al. [49] first enhanced the nuclei according to the features of the images, then employed the morphological reconstruction and geometric features to screen out the nuclei. Kaur et al. [50] combined a multi-scale top hat filter and h-maxima to improve the contrast of the images and further adopted a curvelet initialized level set method to detect nuclei boundaries. Vigueras-Guillen et al. [51] used support vector machines (SVM) for segmenting low contrast corneal endothelium images. Wang et al. [52] proposed a nuclei segment qualifier based on convolutional neural network (CNN) and the linear iterative clustering superpixel method to deal with the low contrast.

1.2. Motivation and contributions

On the basis of learning and summarizing the results of previous studies, we propose an automatic method for cervical nuclei segmentation from cell clusters directly. It aims to improve the accuracy of cell nucleus segmentation and simplify the working process.

The contributions of this paper are as follows:

1. SEENS effectively integrates selective search to segment large cervical cell images into multiple small ROI automatically, which not only eliminates the process of manually clipping large images, but also simplifies multiple objects segmentation into single object segmentation, thereby reducing the subsequent fine segmentation difficulty.
2. To the best of our knowledge, SEENS is the first proposal to apply double screening in ROI selections to avoid repeated segmentation and improve segmentation performance.

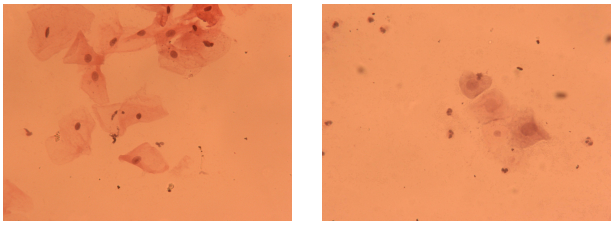

(a) (b)

Figure 1: Cervical smear images containing multiple overlapping cell clusters (a) Cell nuclei with high contrast (b) Cell nuclei with low contrast

3. SEENS improves the segmentation results of the cell images in low contrast scenarios.
4. We have collaborated with medical professionals in establishing a real-world clinical data set, with thorough ground-truth labeling.

The rest of this paper is organized as follows. Section 2 introduces the proposed method. In Section 3, experimental results are presented and analyzed. This paper is summarized in Section 4.

2. Framework For Cervical Nuclei Segmentation

In clinical practice, smear images used for cervical cancer screening may contain single or multiple independent cells or multiple overlapping cells. For multiple overlapping cells, especially for clusters containing a large number of cells (as shown in Fig. 1), nucleus segmentation is the basic and important step of cervical cancer screening based on quantitative analysis of nuclear morphology. At present, improving the accuracy of nucleus segmentation is still an open topic in the study of cervical multi-cell segmentation.

For nucleus fine segmentation in multiple overlapping cell clusters, a novel segmentation model of cervical nuclei is proposed for the first time combined with selective search, mathematical morphology, canny operator and the Chan-Vese (CV) model. Fig. 2 shows the block diagram of cervical nuclei segmentation, which mainly consists of three major processes: A. ROI extraction; B. ROI screening; C. Nucleus segmentation.

First, ROIs potentially containing a nucleus or nuclei are extracted from the background by the selective search, and then subsequent steps are performed on every extracted ROI. It can avoid segmenting numerous nuclei directly in the whole image with complex background and low contrast, thereby reducing the complication of nucleus segmentation. In this way, it transforms the multi-object segmentation into several simpler single-object segmentation processes. After that, the primary ROIs are screened two times in order to remove repeated selection regions and non-nucleus regions, consequently improving the efficiency of nuclei segmentation to a certain extent. Finally, based on contrast grouping, the ROIs in the lower contrast group are first edge-enhanced and then segmented by the CV model, while those in higher contrast group are directly segmented by the CV model. The Canny operator combined with mathematical morphology is used to extract the edge information in order to enhance the original nucleus ROI to be segmented, consequently increasing the segmentation accuracy of the CV model. The screening algorithm is outlined in Algorithm 1.

2.1. ROI Extraction

Generally, in the original Pap smear image, the cells are contaminated by various tissues or impurities and other cells or uneven background color distribution, which all bring interference to the cervical cell image segmentation. Therefore, it is difficult to use a global segmentation algorithm for segmenting whole nucleus from each cell area. Because of this difficulty, selective search segmentation is used to automatically segment the whole image into multiple regions, each of which might contain a nucleus or nuclei. It essentially transforms global segmentation into local segmentation, and each local segmentation process does not affect each other. In other words, subsequent operations are carried out on each ROI, simplifying multiple objects segmentation into single object segmentation. Naturally, the segmentation becomes less difficult.

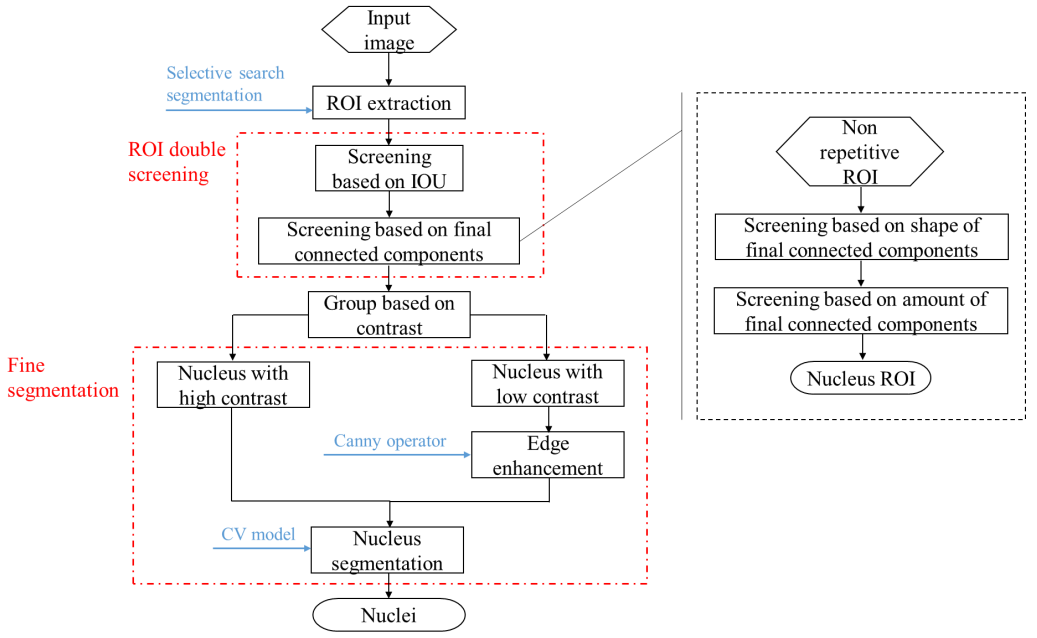

Figure 2: Block diagram of cervical nuclei segmentation

Selective search was first proposed by Uijlings et al. [53] for object recognition, which was used to extract ROI for object recognition, that is, finding an object and locating it in an image. Compared with exhaustive search, selective search is less computationally-intensive. In other words, it takes less time to process the same picture. In order to get bounding boxes that adapt to varied-size objects, exhaustive search needs to change the size of the window and scan the entire image multiple times, while selective search combines a graph-based image segmentation algorithm with a hierarchical algorithm to fuse regions based on the similarity between the initial segments [53]. Selective search is more suitable for segmenting large size cervical cell images with different shapes and sizes of nuclei.

In previous cervical cell nuclear segmentation studies, the nucleus regions to be segmented were obtained by multiple manual interception. In contrast, selective search segmentation can automatically extract regions potentially containing nucleus with different sizes from the whole image (as shown in Fig. 3) and abandon non-nucleus area without manual operation.

2.2. ROI Screening

In order to avoid missing the nucleus region, the selective search segmentation parameters should be over-adjusted, which may result in the repeated extraction of the same region and non-nucleus region extraction. Therefore, double screening is required to remove the repeated selection regions and non-nucleus regions, and only retain the ROI containing the nucleus.

2.2.1. Screening based on intersection over union

The screening of repeated selection regions consists of two steps: 1) determining whether the two regions overlap, 2) calculating the IOU between the two overlapping regions and judging whether the IOU is higher than a threshold. If so, the larger overlapping region will be retained. The IOU is defined by:

$$IOU = \frac{s(ROI_{p_i} \cap ROI_{p_j})}{s(ROI_{p_i} \cup ROI_{p_j})} = \frac{s(ROI_{p_i} \cap ROI_{p_j})}{s(ROI_{p_i}) + s(ROI_{p_j}) - s(ROI_{p_i} \cap ROI_{p_j})}, \tag{1}$$

where ROI_{p_i} and ROI_{p_i} represent the ith and the jth primary ROIs, respectively and $s(\cdot)$ represents the area.

Algorithm 1: Pseudo-code for double screening nuclei segmentation

Input: Whole slide Pap smear image I
Output: Individual nucleus N_c
ROI extraction:
1) Initial regions $R = \{r_1, \ldots, r_n\}$ using graph-based image segmentation
2) Calculate similarity between neighboring regions(r_i, r_j)
3) Merge regions with high similarity into a new region
4) Extract object location boxes as primary ROI: $ROI_p = \left\{ ROI_{p_1}, \ldots, ROI_{p_m} \right\}$
ROI screening:
1) Sort the primary ROIs from large to small according to area
2) Calculate the Intersection over Union (IOU) between ROI_{p_i} and ROI_{p_j}
3) Record index $j \in J$
for *i from* 1 *to m* **do**
  for *j from* $i+1$ *to m* **do**
    if ROI_{p_i} *and* ROI_{p_j} *overlap* **then**
      calculate IOU between ROI_{p_i} and ROI_{p_j};
      if $IOU \geq a$ *(a threshold)* **then**
        record index $j \in J$;
4) Remove overlapping regions, index $j \in J$. Update retained ROI as first screening ROI:
$ROI_{fs} = \left\{ ROI_{fs_1}, \ldots, ROI_{fs_z} \right\}$
5) Process ROI_{fs_k} by ultimate erosion to get final connected components
6) Save ROI according the shape and number of final connected components as second screening ROI:
$ROI_{ss} = \left\{ ROI_{ss_1}, \ldots, ROI_{ss_p} \right\}$
Nucleus segmentation:
for $l = 1 : p$ **do**
  Calculate contrast of $ROI_{ss_l}(C_R)$;
  if $C_R \leq b$ *(a threshold)* **then**
    Extract edge information by the Canny operator combined with mathematical morphology;
    Enhance ROI_{ss_l} by edge information;
  else goto Final
Final: Segment ROI_{ss_l} by the CV model

2.2.2. Screening based on final connected components

For the screening of non-nucleus regions, we use ultimate erosion of mathematical morphology to get the final connected components of ROI. The final connected components of nucleus ROI and non-nucleus ROI are shown in Figs. 4(a) and 4(b), respectively. The final connected components of nucleus are generally concentrated in the middle of the image, while those of non-nucleus are scattered and irregular. Besides, the area of final connected components of the nucleus is smaller than that of the non-nucleus. According to the distribution and quantity of the final connected components, the nucleus ROI can be effectively screened and retained.

2.3. Nucleus Segmentation

The Chan-Vese (CV) algorithm [54] is suitable to segment a medical image whose boundaries are not necessarily discontinuous. However, cervical cell images typically have abnormally-high noise and the low contrast. Therefore, the robustness of the CV model segmentation for cervical cell images is not high enough. Hence, before the fine segmentation, the nucleus ROIs are divided into two groups: a high contrast group and a low contrast group, based on different gray histograms. It is because the distribution of the gray histogram can reflect the contrast of an image, as shown in Fig. 5. The lower the contrast is, the narrower the histogram will be. After grouping, the nucleus with high contrast is directly segmented by the CV model, while the low contrast nucleus needs to be edge-enhanced first and then

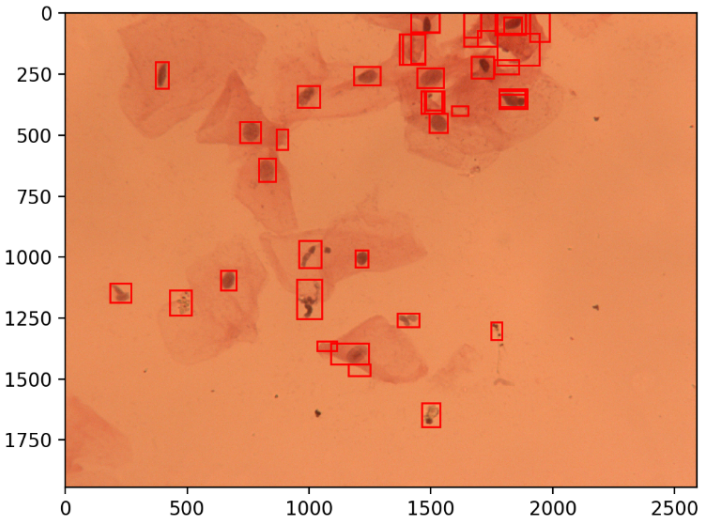

Figure 3: ROI with different size extracted by selective search

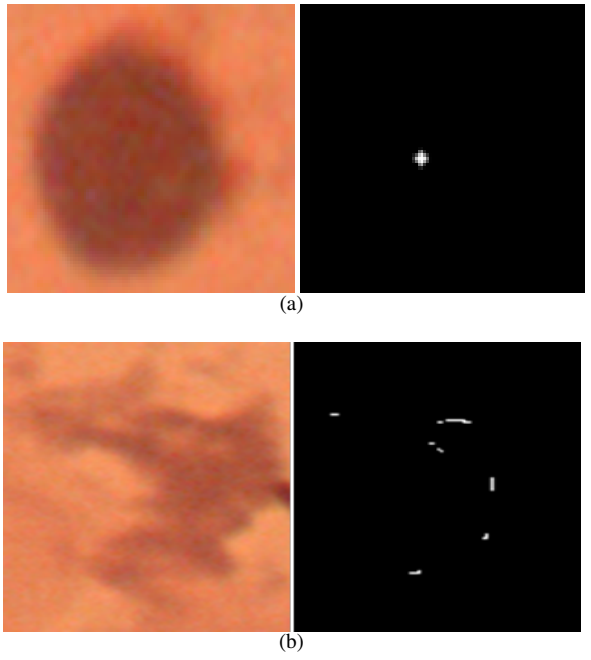

Figure 4: Comparison of final connected components. (a) the nucleus region and its final connected components. (b) the non-nucleus region and its final connected components.

segmented. Combined with mathematical morphology, the Canny operator [55] is used to extract edge information to enhance the image to be segmented so as to improve the accuracy and robustness of the segmentation results of CV model.

For the cervical cell images with high noise interference, the edge information extracted by the Canny operator not only includes the edge of the nucleus, but also false edges caused by noise. In order to remove false edges, mathematical morphological operations and logical operations are used to process the nucleus image to be segmented. The specific

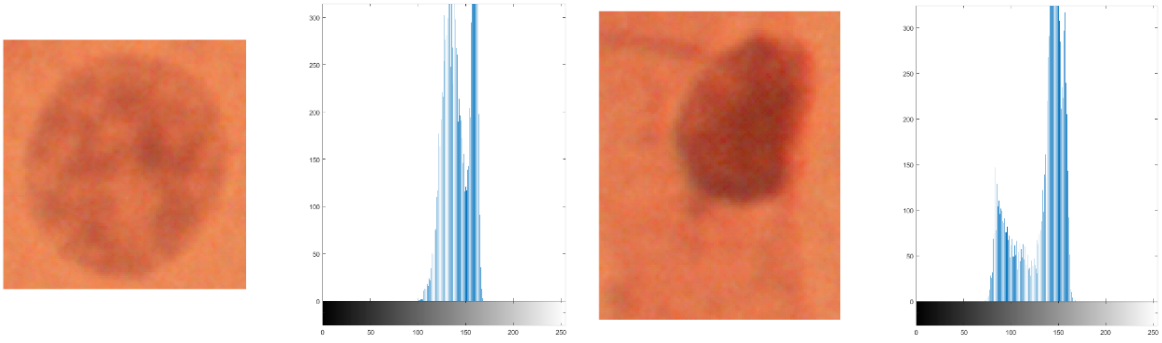

(a) (b)

Figure 5: Comparison of gray histogram distributions. (a) low contrast image and its gray histogram. (b) high contrast image and its gray histogram.

Figure 6: The nucleus region and its edge information. From left to right: the nucleus region; the edge information extracted by the Canny operator; the nucleus edges.

steps are as follows: Step 1) the Canny operator is used to extract all the edge information of the nucleus ROI, denoted by M_{canny} as shown in Fig. 6; Step 2) Binarization is used to process the nucleus ROI to obtain $M_{binarization}$; Step 3) Dilatation is used to process $M_{binarization}$ to get $M_{dilatation}$; Step 4) Erosion is used to process $M_{dilatation}$ to get $M_{erosion}$; Step 5) the logical operation is performed, and the result is denoted by M_{edge}, as shown below,

$$M_{edge} = M_{canny} \& M_{dialation} \& \overline{M}_{erosion}. \tag{2}$$

That is the edge of the nucleus, as shown in Fig. 6.

Although the extracted edge information of the nucleus is not continuous, it still can be used as a weight to be added to the original image to enhance its edge, especially for weak edges. After edge enhancement, the segmentation accuracy of the CV model is improved, as shown in Fig. 7.

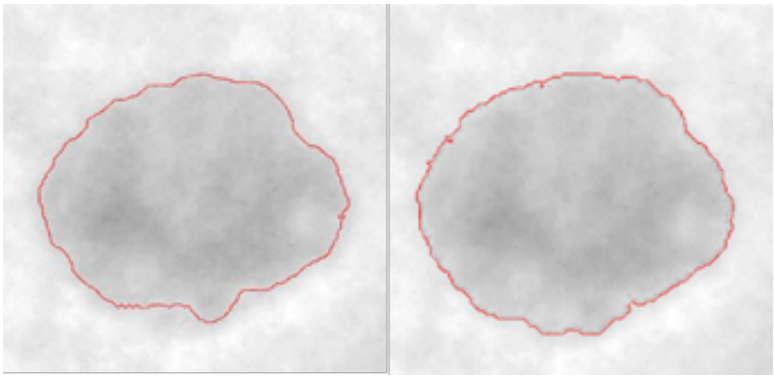

Figure 7: The nucleus region and its edge information. Left: Segmentation result of the CV model without edge enhancement; Right: Segmentation result of the CV model with edge enhancement.

3. Results and Discussion

3.1. ROI Extration and Nuclei Screening

All experiments in this paper were conducted on actual patients' Pap smear images with suspected lesions from Tianjin Tumor Hospital affiliated with Tianjin Medical University. Each image size is 2592×1944 pixels. There are 18 whole slide cervical cell images from different individuals and quantified the experimental results, as summarized in Table 1. The robustness of the proposed method is evaluated by false rate and missed rates of ROI extraction and screening. Because missed selection of nucleus has a large effect on quantitative analysis of nucleus morphology, the accuracy of ROI extraction and screening is measured by the missed rate and the false rate, which are defined as follows, respectively,

$$\text{Missed Rate} = \frac{\text{Missed Selection}}{\text{Total Nuclei Number}}, \tag{3}$$

$$\text{False Rate} = \frac{\text{False Selection}}{\text{Total Nuclei Number}}. \tag{4}$$

In addition, the accuracy is defined as follows,

$$\text{Accuracy} = 1 - \text{Missed Rate}. \tag{5}$$

We have analyzed the sources of the errors: For nucleus false detection usually occurs when there are blood clots or excessive staining tissues in the cervical cell images, especially when those interference shapes are similar to nucleus; As for the causes of missed detection are diverse since it is often caused by uneven background dyeing and influenced by the choice of parameter settings.

Due to the uneven staining of cervical smears, the contrast between the nuclei and the background in each cervical smear image varies. Experimental results of three representative images with different contrast are presented as follows. It is shown that the primary ROI can be effectively extracted from different contrast images by selective search (Fig. 8(a), Fig. 9(a), Fig. 10(a)). Then, the primary ROIs are screened twice, and the selected ROIs are shown in Fig. 8(b), Fig. 9(b) and Fig. 10(b), respectively. The experimental results show that the proposed method has high accuracy in extraction and screening of ROIs.

3.2. Contrast Evaluation

After ROI extraction, 399 ROI regions are selected, and with ROI screening, 20 false selection (non-nuclei regions) are removed. Therefore, in total, 379 nuclei are used for the contrast evaluation and further fine segmentation. In image ID 1 (Fig. 8), the contrast values of indexes 1, 5, 6 nucleus are higher than those of the others. Almost every nucleus in image ID 2 (Fig. 9) have lower contrast, while those in image ID 8 (Fig. 10) are higher. As shown in the figures,

Table 1
ROI extraction and screening performance for 18 wholde slide images

Image ID	Nuclei Number	ROI Number	Missed Selection	False Selection	Missed Rate	False Rate	Accuracy
1	7	7	0	0	0	0	100%
2	12	12	0	0	0	0	100%
3	17	18	0	1	0	5.9%	100%
4	22	23	1	2	4.5%	9.1%	95.5%
...	...	...	...	...	...	...	...
17	49	51	1	3	2.0%	6.1%	98%
18	19	20	0	1	0	5.3%	100%
total	**395**	**399**	**16**	**20**	**4.1%**	**5.1%**	**95.9%**

selective search is applicable to Pap smear images with different contrast or uneven contrast when the two parameters (scale and size) are adjusted. After a number of experiments, it can be determined that the parameter scale ranges from 100 to 300, with 50 as an adjustment unit and the parameter size ranges from 15 to 50, with 5 as an adjustment unit.

3.3. Edge Enhancement and Nuclei Segmentation

After grouping the extracted and screened ROI according to the contrast (with 158 low contrast nuclei and 221 high contrast nuclei), CV model and CV model after edge enhancement are used for fine segmentation of the two groups with different contrast values, respectively. For the high contrast nucleus ROI the CV model can segment the nucleus well. Fig. 11 shows a part of the segmentation results of the CV model. While for the low contrast nucleus ROI, the segmentation accuracy of the CV model is not high enough. In order to show the results of the proposed method more intuitively, we plot the representative segmentation results after 500 iterations of the CV model in contrast to the proposed method as shown in Fig. 12. Experimental results show that the segmented boundaries of the nuclei without enhancement are non-continuous, even with some non-accurately segmented area. While after enhancement, better segmentation performance is achieved.

Different contrast images correspond to different gray histogram distributions. Accordingly, selecting a proper threshold for grouping nucleus ROI to be segmented and then only enhancing the ROI in the low contrast group can effectively improve the efficiency of the cell segmentation. The experimental results show that the appropriate threshold range is from 80 to 85. Besides, according to the segmentation results in Fig 11 and Fig. 12, the proposed method can improve the segmentation accuracy of low contrast nucleus.

3.4. Segmentation Evaluation and Discussion

We present a non-learning segmentation method which requires no user intervention and no human labeling for the training of models. The method provides satisfying results in cell nuclei segmentation from whole slide Pap smear images. To further demonstrate the effectiveness our method, we label 50 cell nuclei (with 25 high contrast and 25 low contrast) to evaluate the segmentation result.

We compare our proposed method with the CV-model without enhancement, Automatic Fuzzy Clustering Framework (AFCF) [12] and Adaptive Morphological Reconstruction (AMR) [13], which are reported to be state-of-the-art non-learning-based segmentation methods. We use Dice, Jaccard, Precision and Recall as evaluation metrics to evaluate the segmentation results. The definitions of these coefficients are as follows.

$$\text{Dice}\left(G,R\right)=2\times\frac{G\cap R}{G+R}=2\times\frac{TP}{TP+FP+TP+FN}\ , \tag{6}$$

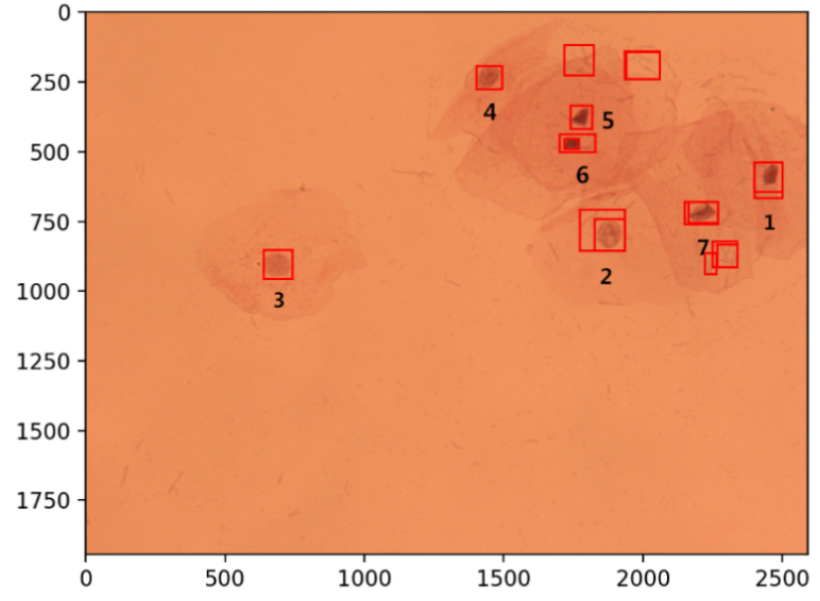

(a)

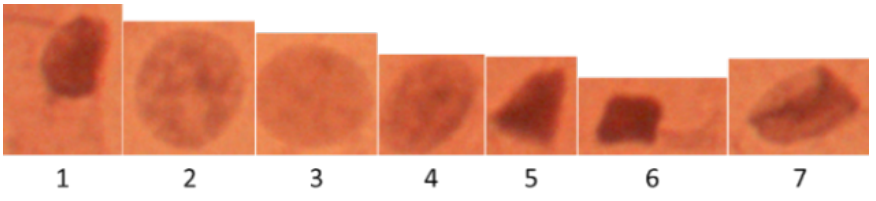

(b)

Figure 8: ROI extraction and screening results of image ID 1. (a) ROI extraction results. (b) ROI screening results. Nucleus ROI in (a) and (b) corresponds to each other according to the indexes.

$$\text{Jaccard} = \frac{G \cap R}{G \cup R} = \frac{TP}{TP + FP + FN}, \tag{7}$$

$$\text{Precision} = \frac{TP}{TP + FP}, \tag{8}$$

$$\text{Recall} = \frac{TP}{TP + FN}, \tag{9}$$

where G represents for the ground-truth and R represents for the result image.

The comparison results are shown in Fig. 13 and Table. 2.

For low contrast nuclei, SEENS achieves the highest results of all four coefficients, while for high contrast nuclei, SEENS has the highest performance in Dice, Jaccard and Recall. For precision, AFCF performs better because AFCF usually segments larger areas than the ground-truth (Fig. 13). Experimental results demonstrate that SEENS has higher performance than AFCF and AMR for nuclei images, with increment of the Dice to be 11% and 21%, respectively. Meanwhile, the Recall increases 14.5% and 15.1%, respectively. Particularly, for low contrast images, SEENS achieves better performances compared with the non-enhanced method, with the Dice increasing 3% and the Recall increasing 4%.

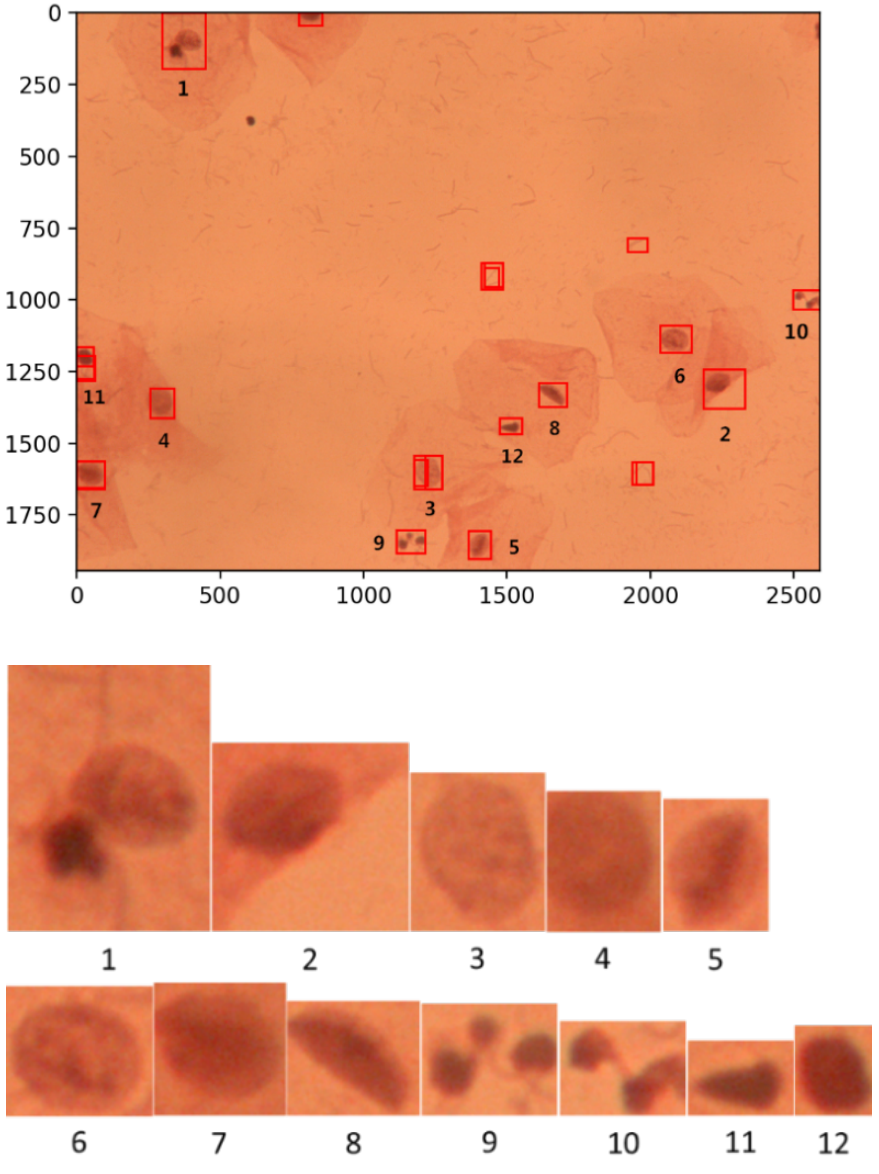

Figure 9: ROI extraction and screening results of image ID 2. (a) ROI extraction results. (b) ROI screening results. Nucleus ROI in (a) and (b) corresponds to each other according to the indexes.

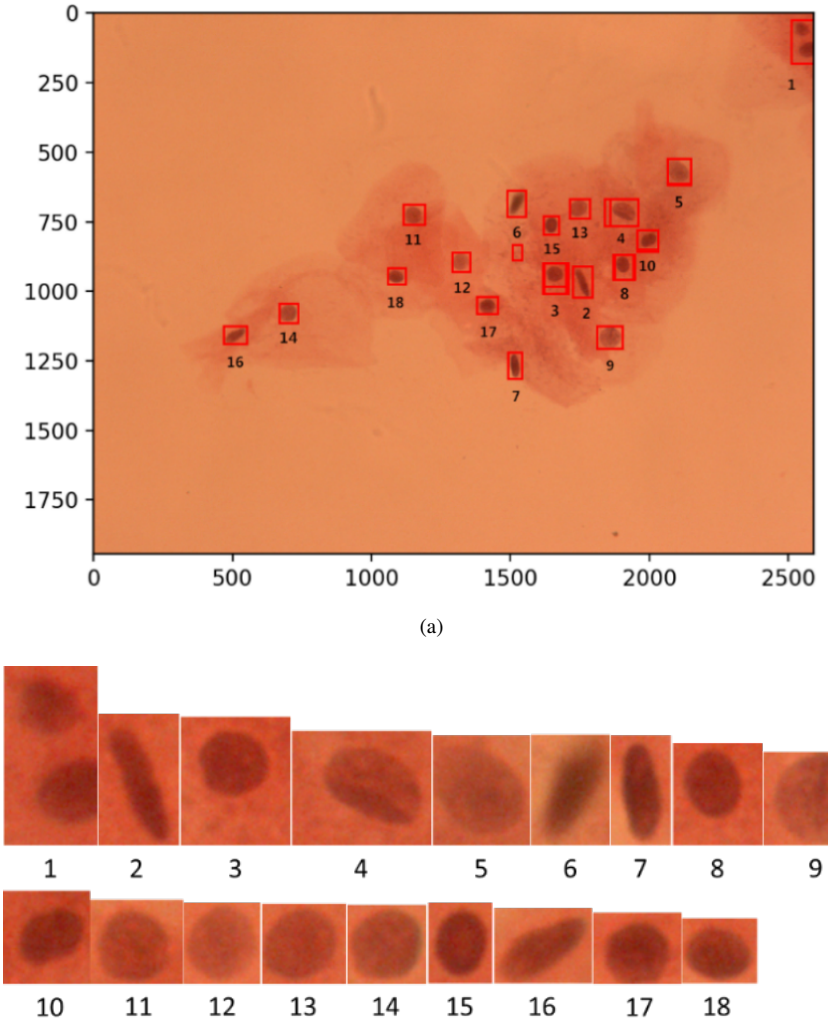

(a)

(b)

Figure 10: ROI extraction and screening results of image ID 8. (a) ROI extraction results. (b) ROI screening results. Nucleus ROI in (a) and (b) corresponds to each other according to the indexes.

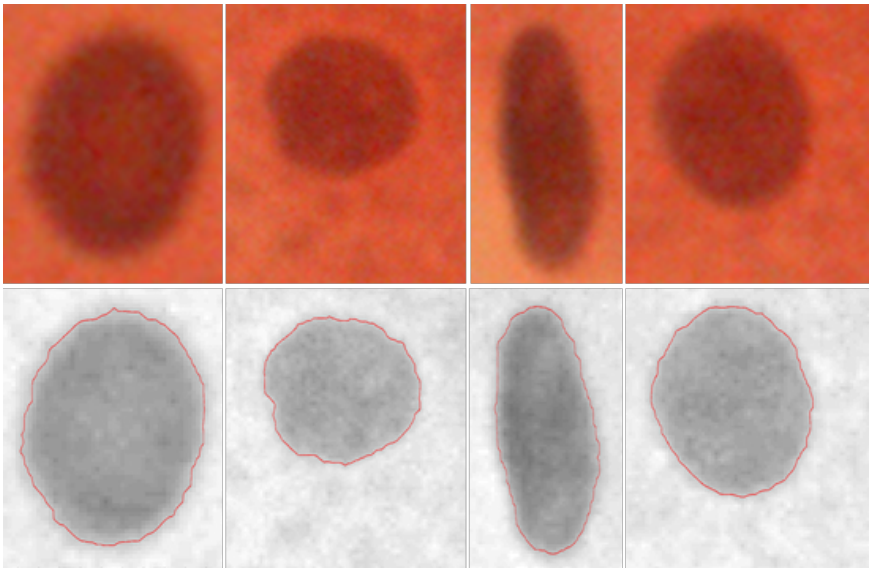

Figure 11: Nuclei with high contrast segmentation results. The first row shows the ROI to be segmented. The second row shows the segmentation results of the CV model. The images are scaled to a certain extent in order to show them clearly.

Table 2
Comparison of the segmentation performance for four algorithms on cell cluster dataset

Group	Method	Dice	Jaccard	Precision	Recall
Low contrast	SEENS	**0.9298**	**0.8708**	**0.9785**	**0.8935**
	without enhancement	0.9073	0.8354	0.9742	0.8535
	AFCF	0.8173	0.7002	0.8709	0.7837
	AMR	no result	no result	no result	no result
High Contrast	SEENS	**0.9447**	**0.8960**	0.9497	**0.9418**
	without enhancement	0.9423	0.8918	0.9457	0.9409
	AFCF	0.8379	0.7365	**0.9627**	0.7620
	AMR	0.7298	0.6491	0.7571	0.7663
Average	SEENS	**0.9373**	**0.8834**	**0.9641**	**0.9177**
	without enhancement	0.9248	0.8636	0.9599	0.8972
	AFCF	0.8276	0.7183	0.9168	0.7728
	AMR	0.7298	0.6491	0.7571	0.7663

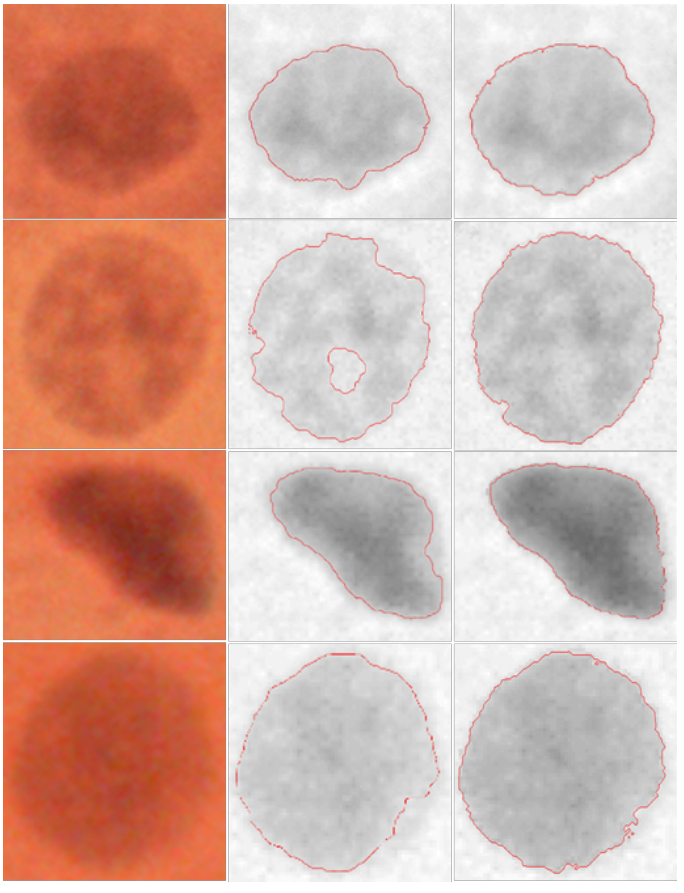

Figure 12: Nuclei with low contrast segmentation results. Column from left to right: ROI to be segmented; segmentation results of the CV model without edge enhancement; segmentation results of the CV model after edge enhancement. The images are scaled to a certain extent in order to show them clearly.

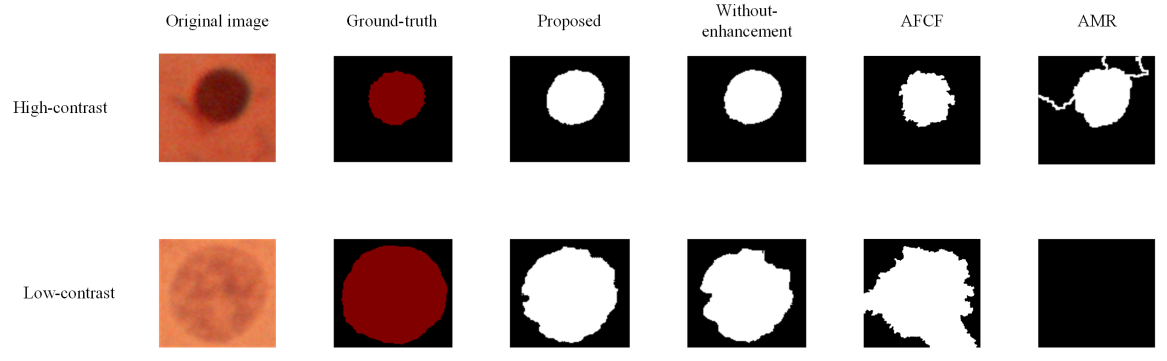

Figure 13: Segmentation Results Compared with Other Methods.

4. Conclusion

In this paper a non-learning-based model–SEENS is proposed to realize accurate segmentation of cell nuclei from whole slide Pap smear images. Most importantly, compared with the CV model, AFCF and AMR, the proposed method improves the segmentation accuracy of nucleus with low contrast and unclear edges. The experimental results demonstrate the robustness and good performance in ROI extraction and nuclei segmentation. Therefore, the proposed method, as a basic while important step of quantitative analysis in nuclear morphology, is quite promising in computer-aided medical diagnosis. Future work will focus on further improving the ROI extraction accuracy and implementing SEENS to be an end-to-end framework. Moreover, more data sets are needed to be labeled to train a learning-based model. We are also exploring different deep learning models for our application.

References

[1] S. Tuli, N. Basumatary, S. S. Gill, M. Kahani, R. C. Arya, G. S. Wander, R. Buyya, Healthfog: An ensemble deep learning based smart healthcare system for automatic diagnosis of heart diseases in integrated iot and fog computing environments, Future Generation Computer Systems 104 (2020) 187–200 (2020).

[2] Z. Pang, G. Yang, R. Khedri, Y.-T. Zhang, Introduction to the special section: convergence of automation technology, biomedical engineering, and health informatics toward the healthcare 4.0, IEEE Reviews in Biomedical Engineering 11 (2018) 249–259 (2018).

[3] H.-N. Dai, R. C.-W. Wong, H. Wang, Z. Zheng, A. V. Vasilakos, Big data analytics for large-scale wireless networks: Challenges and opportunities, ACM Computing Surveys (CSUR) 52 (5) (2019) 99 (2019).

[4] C. Choi, F. Piccialli, J. J. Jung, Internet of knowledge, Future Generation Computer Systems 102 (2020) 948 – 949 (2020).

[5] J. Lu, E. Song, A. Ghoneim, M. Alrashoud, Machine learning for assisting cervical cancer diagnosis: An ensemble approach, Future Generation Computer Systems (2020).

[6] G. Hinton, Y. LeCun, Y. Bengio, Deep learning, Nature 521 (7553) (2015) 436–444 (2015).

[7] G. Casolla, S. Cuomo, V. S. d. Cola, F. Piccialli, Exploring unsupervised learning techniques for the internet of things, IEEE Transactions on Industrial Informatics 16 (4) (2020) 2621–2628 (April 2020).

[8] X. Wang, L. T. Yang, Y. Wang, L. Ren, M. J. Deen, Adtt: A highly-efficient distributed tensor-train decomposition method for iiot big data, IEEE Transactions on Industrial Informatics (2020). doi:10.1109/TII.2020.2967768.

[9] X. Wang, L. T. Yang, L. Song, H. Wang, L. Ren, J. Deen, A tensor-based multi-attributes visual feature recognition method for industrial intelligence, IEEE Transactions on Industrial Informatics (2020). doi:10.1109/TII.2020.2999901.

[10] L. G. Koss, Cervical (pap) smear: new directions, Cancer 71 (S4) (1993) 1406–1412 (1993).

[11] A. Ghoneim, G. Muhammad, M. S. Hossain, Cervical cancer classification using convolutional neural networks and extreme learning machines, Future Generation Computer Systems 102 (2020) 643–649 (2020).

[12] T. Lei, P. Liu, X. Jia, X. Zhang, H. Meng, A. K. Nandi, Automatic fuzzy clustering framework for image segmentation, IEEE Transactions on Fuzzy Systems (2019) 1–1 (2019).

[13] T. Lei, X. Jia, T. Liu, S. Liu, H. Meng, A. K. Nandi, Adaptive morphological reconstruction for seeded image segmentation, IEEE Transactions on Image Processing 28 (11) (2019) 5510–5523 (2019).

[14] Z. Wang, H. Li, Generalizing cell segmentation and quantification, BMC bioinformatics 18 (1) (2017) 189 (2017).

[15] Z. Wang, Cell segmentation for image cytometry: Advances, insufficiencies, and challenges, Cytometry Part A 95 (7) (2019) 708–711 (2019).

[16] P. Wang, X. Hu, Y. Li, Q. Liu, X. Zhu, Automatic cell nuclei segmentation and classification of breast cancer histopathology images, Signal Processing 122 (2016) 1–13 (2016).

[17] O. Sarrafzadeh, A. M. Dehnavi, Nucleus and cytoplasm segmentation in microscopic images using k-means clustering and region growing, Advanced biomedical research 4 (2015).

[18] F. Xing, L. Yang, Robust nucleus/cell detection and segmentation in digital pathology and microscopy images: a comprehensive review, IEEE reviews in biomedical engineering 9 (2016) 234–263 (2016).

[19] Y. Song, E.-L. Tan, X. Jiang, J.-Z. Cheng, D. Ni, S. Chen, B. Lei, T. Wang, Accurate cervical cell segmentation from overlapping clumps in pap smear images, IEEE transactions on medical imaging 36 (1) (2016) 288–300 (2016).

[20] P. J. Schüffler, D. Schapiro, C. Giesen, H. A. Wang, B. Bodenmiller, J. M. Buhmann, Automatic single cell segmentation on highly multiplexed tissue images, Cytometry Part A 87 (10) (2015) 936–942 (2015).

[21] A. Tareef, Y. Song, H. Huang, D. Feng, M. Chen, Y. Wang, W. Cai, Multi-pass fast watershed for accurate segmentation of overlapping cervical cells, IEEE transactions on medical imaging 37 (9) (2018) 2044–2059 (2018).

[22] M. Gamarra, E. Zurek, H. J. Escalante, L. Hurtado, H. San-Juan-Vergara, Split and merge watershed: A two-step method for cell segmentation in fluorescence microscopy images, Biomedical Signal Processing and Control 53 (2019) 101575 (2019).

[23] S. Khobragade, D. D. Mor, C. Patil, Detection of leukemia in microscopic white blood cell images, in: 2015 International Conference on Information Processing (ICIP), IEEE, 2015, pp. 435–440 (2015).

[24] C. Molnar, I. H. Jermyn, Z. Kato, V. Rahkama, P. Östling, P. Mikkonen, V. Pietiäinen, P. Horvath, Accurate morphology preserving segmentation of overlapping cells based on active contours, Scientific reports 6 (2016) 32412 (2016).

[25] T.-H. Song, V. Sanchez, H. EIDaly, N. M. Rajpoot, Dual-channel active contour model for megakaryocytic cell segmentation in bone marrow trephine histology images, IEEE Transactions on Biomedical Engineering 64 (12) (2017) 2913–2923 (2017).

[26] J. Liu, H. Jung, A. Dubra, J. Tam, Cone photoreceptor cell segmentation and diameter measurement on adaptive optics images using circularly constrained active contour model, Investigative ophthalmology & visual science 59 (11) (2018) 4639–4652 (2018).

[27] W. Zhang, H. Li, Automated segmentation of overlapped nuclei using concave point detection and segment grouping, Pattern Recognition 71 (2017) 349–360 (2017).
[28] R. Rojas-Moraleda, W. Xiong, N. Halama, K. Breitkopf-Heinlein, S. Dooley, L. Salinas, D. W. Heermann, N. A. Valous, Robust detection and segmentation of cell nuclei in biomedical images based on a computational topology framework, Medical image analysis 38 (2017) 90–103 (2017).
[29] N. Reljin, M. Slavkovic-Ilic, C. Tapia, N. Cihoric, S. Stankovic, Multifractal-based nuclei segmentation in fish images, Biomedical microdevices 19 (3) (2017) 67 (2017).
[30] M. Unser, Texture classification and segmentation using wavelet frames, IEEE Transactions on image processing 4 (11) (1995) 1549–1560 (1995).
[31] P.-M. Juneau, A. Garnier, C. Duchesne, Monitoring of adherent live cells morphology using the undecimated wavelet transform multivariate image analysis (uwt-mia), Biotechnology and bioengineering 114 (1) (2017) 141–153 (2017).
[32] L. Caponetti, G. Castellano, M. T. Basile, V. Corsini, Fuzzy mathematical morphology for biological image segmentation, Applied intelligence 41 (1) (2014) 117–127 (2014).
[33] A. Loddo, C. Di Ruberto, M. Kocher, Recent advances of malaria parasites detection systems based on mathematical morphology, Sensors 18 (2) (2018) 513 (2018).
[34] X. Chen, Y. Zhu, F. Li, Z.-Y. Zheng, E. C. Chang, J. Ma, S. T. Wong, Accurate segmentation of touching cells in multi-channel microscopy images with geodesic distance based clustering, Neurocomputing 149 (2015) 39–47 (2015).
[35] L. Dudakova, S.-S. Cheong, S. R. Merjava, P. Skalicka, M. Michalickova, M. Palos, G. Mahelkova, D. Krizova, M. Hlozanek, M. Trkova, et al., Familial limbal stem cell deficiency: clinical, cytological and genetic characterization, Stem Cell Reviews and Reports 14 (1) (2018) 148–151 (2018).
[36] O. Ronneberger, P. Fischer, T. Brox, U-net: Convolutional networks for biomedical image segmentation, in: International Conference on Medical image computing and computer-assisted intervention, Springer, 2015, pp. 234–241 (2015).
[37] E. Moen, D. Bannon, T. Kudo, W. Graf, M. Covert, D. Van Valen, Deep learning for cellular image analysis, Nature methods (2019) 1–14 (2019).
[38] T. Wollmann, M. Gunkel, I. Chung, H. Erfle, K. Rippe, K. Rohr, Gruu-net: Integrated convolutional and gated recurrent neural network for cell segmentation, Medical image analysis (2019).
[39] Y. Liu, F. Cao, J. Zhao, J. Chu, Segmentation of white blood cells image using adaptive location and iteration, IEEE journal of biomedical and health informatics 21 (6) (2016) 1644–1655 (2016).
[40] X. Bai, C. Sun, C. Sun, Cell segmentation based on fopso combined with shape information improved intuitionistic fcm, IEEE journal of biomedical and health informatics 23 (1) (2018) 449–459 (2018).
[41] M. E. Plissiti, C. Nikou, A. Charchanti, Automated detection of cell nuclei in pap smear images using morphological reconstruction and clustering, IEEE Transactions on information technology in biomedicine 15 (2) (2010) 233–241 (2010).
[42] L. Zhang, M. Sonka, L. Lu, R. M. Summers, J. Yao, Combining fully convolutional networks and graph-based approach for automated segmentation of cervical cell nuclei, in: 2017 IEEE 14th international symposium on biomedical imaging (ISBI 2017), IEEE, 2017, pp. 406–409 (2017).
[43] M. E. Plissiti, C. Nikou, A. Charchanti, Combining shape, texture and intensity features for cell nuclei extraction in pap smear images, Pattern Recognition Letters 32 (6) (2011) 838–853 (2011).
[44] N. Byju, V. K. Sujathan, P. Malm, R. R. Kumar, A fast and reliable approach to cell nuclei segmentation in pap stained cervical smears, CSI transactions on ICT 1 (4) (2013) 309–315 (2013).
[45] Y. Song, L. Zhang, S. Chen, D. Ni, B. Lei, T. Wang, Accurate segmentation of cervical cytoplasm and nuclei based on multiscale convolutional network and graph partitioning, IEEE Transactions on Biomedical Engineering 62 (10) (2015) 2421–2433 (2015).
[46] I. Muhimmah, R. Kurniawan, Indrayanti, Automated cervical cell nuclei segmentation using morphological operation and watershed transformation, in: 2012 IEEE International Conference on Computational Intelligence and Cybernetics (CyberneticsCom), 2012, pp. 163–167 (July 2012).
[47] Chin-Wen Chang, Ming-Yu Lin, Horng-Jyh Harn, Yen-Chern Harn, Chien-Hung Chen, Kun-His Tsai, Chi-Hung Hwang, Automatic segmentation of abnormal cell nuclei from microscopic image analysis for cervical cancer screening, in: 2009 IEEE 3rd International Conference on Nano/Molecular Medicine and Engineering, 2009, pp. 77–80 (Oct 2009).
[48] L. Zhang, H. Kong, C. T. Chin, S. Liu, Z. Chen, T. Wang, S. Chen, Segmentation of cytoplasm and nuclei of abnormal cells in cervical cytology using global and local graph cuts, Computerized Medical Imaging and Graphics 38 (5) (2014) 369 – 380 (2014).
[49] T. Guan, D. Zhou, W. Fan, K. Peng, C. Xu, X. Cai, Nuclei enhancement and segmentation in color cervical smear images, in: 2014 IEEE International Conference on Robotics and Biomimetics (ROBIO 2014), 2014, pp. 107–112 (2014).
[50] S. Kaur, J. S. Sahambi, Curvelet initialized level set cell segmentation for touching cells in low contrast images, Computerized Medical Imaging and Graphics the Official Journal of the Computerized Medical Imaging Society 49 (2016) 46–57 (2016).
[51] J. P. Vigueras-Guillén, E. R. Andrinopoulou, A. Engel, H. G. Lemij, J. V. Rooij, K. A. Vermeer, L. J. V. Vliet, Corneal endothelial cell segmentation by classifier-driven merging of oversegmented images, IEEE Transactions on Medical Imaging 37 (10) (2018) 2278–2289 (2018).
[52] R. Wang, S.-I. Kamata, Nuclei segmentation of cervical cell images based on intermediate segment qualifier, in: International Conference on Pattern Recognition, 2018 (2018).
[53] J. R. Uijlings, K. E. Van De Sande, T. Gevers, A. W. Smeulders, Selective search for object recognition, International journal of computer vision 104 (2) (2013) 154–171 (2013).
[54] T. F. Chan, L. A. Vese, Active contours without edges, IEEE Transactions on image processing 10 (2) (2001) 266–277 (2001).
[55] J. Canny, A computational approach to edge detection, IEEE Transactions on pattern analysis and machine intelligence (6) (1986) 679–698 (1986).